A detailed study of crosswind effects on train systems

Chris Baker

Abstract

This report presents a detailed analysis of the effects of unsteady crosswinds on trains using a simple train dynamic system methodology. This begins with the specification of unsteady wind characteristics that are then used to calculate unsteady aerodynamic forces. These are then used as input to the dynamic model to calculate lateral, vertical and rotational displacements and unsteady track forces. Three specific effects are then considered – wheel unloading criteria, track force criteria and vehicle displacement criteria, and a rigorous statistical methodology used to specify values of these under specific unsteady crosswind conditions. A simple methodology for developing wheel unloading cross wind characteristics (CWCs) is then set out and calibrated using the dynamic model. This calibration indicates that the simple model is more than adequate to determine wheel unloadings, and that the more complex aspects of the suspension, track roughness of spatial non-correlation of the aerodynamic loads have little effect on the calculated CWCs. Finally possible extensions to the modelling methodology are outlined – in terms of investigating a range of effects on wheel unloading dynamics, the extension of the method to investigate track forces, roof displacements and pantograph / OHL displacements in cross winds.

Notation

A	Train reference area (m^2)
A_x	Roughness parameter (mrad)
A_y	Roughness parameter (mrad)
c	Characteristic velocity for wheel unloading limit (m/s)
c_X	Characteristic velocity for roof displacement limit (m/s)
c_μ	Characteristic velocity for Nadal limit (m/s)
$c_{s\theta}$	Secondary rotational damping (Nms/rad)
c_{sx}	Secondary lateral damping (kg/s)
c_{sy}	Secondary vertical damping (kg/s)
C	Track curvature (m^{-1})
C_L	Lift force coefficient
C_R	Rolling moment coefficient about rollcentre
C_{RL}	Lee rail rolling moment coefficient
C_S	Side force coefficient
$C_L(\psi)$	Lift force coefficient at yaw angle ψ
$C_{RL}(\psi)$	Rolling moment coefficient at yaw angle ψ
$C_S(\psi)$	Side force coefficient at yaw angle ψ
d_α	Dispersion of wheel loading coefficient extreme value distribution
d_β	Dispersion of Nadal coefficient extreme value distribution
d_γ	Dispersion of lateral displacement coefficient extreme value distribution
f_a	Admittance factor
f_c	Curvature factor $\left(\left(\frac{v_b}{v}\right)^2 - 1\right)\frac{qCv^2}{pg}$
f_r	Roughness factor
f_{s1}	Suspension rotation factor $1 - \epsilon s$
f_{s2}	Suspension lateral movement factor $\frac{M_{pr}}{M_t}\frac{x_{pr}}{p} + \frac{M_{se}}{M_t}\frac{x_{se}}{p}$
f_{s3}	Suspension other effects factor
h	Reference height (m)
$h_L(\tau)$	Lift force weighting function
$h_S(\tau)$	Side force weighting function

H	Horizontal force on track (N)
I_s	Moment of inertia of secondary suspended mass (kg m^2)
k_{px}	Primary lateral stiffness (N/m)
k_{py}	Primary vertical stiffness (N/m)
k_{sx}	Secondary lateral stiffness (N/m)
k_{sy}	Secondary vertical stiffness (N/m)
$k_{s\theta}$	Secondary rotational stiffness (Nm/rad)
l	Vehicle length (m)
$\bar{L}$	Mean lift force (N)
L'	Fluctuating lift force (N)
L_u	Turbulence length scale relative to the vehicle (m)
L_{xu}	Actual turbulence length scale (m)
m_L	Lift force weighting function parameter
m_S	Side force weighting function parameter
m_α	Mode of wheel loading coefficient extreme value distribution
$m_{\alpha i}$	Values of m_α used in the analysis of section 12.
m_γ	Mode of lateral displacement coefficient extreme value distribution
m_μ	Mode of Nadal coefficient extreme value distribution
M_p	Primary suspended mass (kg)
M_s	Secondary suspended mass (kg)
M_{sp}	Total suspended mass (kg)
M_t	Total vehicle mass (kg)
M_u	Unsprung mas (kg)
n	Frequency (Hz)
n_j	Frequency at increment *j* (Hz)
n_{L1}	Lift force coefficient low yaw angle exponent
n_{L2}	Lift force coefficient high yaw angle exponent
n_{R1}	Lee rail rolling moment coefficient low yaw angle exponent
n_{R2}	Lee rail rolling moment high yaw angle exponent
n_{S1}	Side force coefficient low yaw angle exponent
n_{S2}	Side force coefficient high yaw angle exponent

N	Number of realisations of dynamic model
p	Track semi-width (m)
P_j	Probability of exceedance
q	Centre of pressure height above leeward rail (m)
q'	Centre of pressure height above roll centre (m)
r_{ij}	Random number between 0 and 1
R	Rolling moment causing secondary rotational displacement (Nm)
R_j	Rank
R_o	Overturning moment (Nm)
R_r	Restoring moment (Nm)
s	Suspension coefficient
s_{sp}	Height of centre of gravity of suspended mass above rail (m)
s_t	Height of centre of gravity of total mass above rail (m)
s'_t	Height of centre of gravity of total mass above roll centre (m)
s_u	Height of centre of gravity of unsprung mass above rail (m)
$\bar{S}$	Mean side force (N)
S'	Fluctuating side force (N)
S_u	Spectral density of wind relative to the vehicle (m^2/s)
$S_x(\omega)$	Spectral density of lateral roughness
$S_y(\omega)$	Spectral density of vertical roughness
$S_\varphi(\omega)$	Spectral density of cross track roughness
u'	Unsteady wind speed (m/s)
u_i	Unsteady wind speed at time step *I* (m/s)
u_o	Gust velocity for a specified wheel unloading (m/s)
$\bar{u}$	Mean wind speed taken to be normal to the direction of travel) (m/s)
v	Vehicle speed (m/s)
v_b	Balancing speed (m/s)
V	Vertical force on track (excluding self-weight) (N)
$\bar{V}$	Mean wind speed relative to the vehicle (m/s)
t	Time (s)
x_p	Primary lateral displacement (m)

$x_{p\,max}$	Primary maximum lateral displacement (m)
x_{ri}	Lateral roughness (m)
x_s	Secondary lateral displacement (m)
$x_{s\,max}$	Secondary maximum lateral displacement (m)
$x_{s\,rot}$	Secondary lateral displacement caused by body rotations (m)
x_t	Lateral movement of centre of gravity of total mass (m)
y_p	Primary vertical displacement (m)
$y_{p\,max}$	Primary maximum vertical displacement (m)
y_{ri}	Vertical roughness (m)
y_s	Secondary vertical displacement (m)
$y_{s\,max}$	Secondary maximum vertical displacement (m)
α	Wheel unloading coefficient
α'	$\alpha - f_{s2} - f_{s3} - f_a - f_r + f_c$
$\alpha_{max,j}$	Maximum value of wheel unloading coefficient for realization *j*
β	Wind direction
γ	Lateral displacement coefficient
ε	Track cant (rad)
ϵ	Coefficient of proportionality in equation 11.9
θ_s	Secondary roll angle (rad)
ψ	Yaw angle (degrees)
μ	Nadal coefficient
ρ	Density of air (kg/m^3)
σ_u	Standard deviation of wind speed (m/s)
τ	Lag time in weighting function (s)
φ_{ri}	Cross track roughness (rad)
ω	Wavenumber
ω_c	Roughness parameter (rad/m)
ω_r	Roughness parameter (rad/m)
ω_s	Roughness parameter (rad/m)

1. Introduction and rationale

In two papers from 2010 and 2013 [1] [2] the author has set out a general methodology for the consideration of the effects of crosswinds on trains. The first of these developed a theoretical model for the unsteady forces on trains and calibrated this methodology using a simple dynamic model of the train suspension system. The second developed a framework for the consideration of trains in high winds and in particular proposed a simple method for the calculation of cross wind characteristics – a plot of accident wind speed against train speed that is used in the train authorization process. The work of both these papers has been taken further in the book on train aerodynamics by the author and his colleagues published in 2019[3].

This paper draws on this work and presents an overall framework for the consideration of crosswinds on trains, at rather more length than would be possible in a published paper. It considers how the forces produced by fluctuating wind forces are modified by the track dynamic system to cause wheel unloading, high track forces and body displacements. The relative importance of a number of physical parameters – suspension characteristics, track roughness, non-correlation of turbulence on the train surface are considered. This leads to further developments in the methodology for calculating cross wind characteristics, which can be applied to a range of cross wind issues other than the one usually addressed – that of train overturning.

Naturally this paper draws heavily on the earlier work. The two papers and the book give extended reviews of the work of other authors in this field, and readers interested in more background information should consult these.

[1] C.J. Baker, 2010, "The simulation of unsteady aerodynamic cross wind forces on trains", Journal of Wind Engineering & Industrial Aerodynamics 98, 88-99, http://dx.doi.org/10.1016/j.jweia.2009.09.006

[2] C J Baker, 2013, "A framework for the consideration of the effects of crosswinds on trains", Journal of Wind Engineering and Industrial Aerodynamics 123, 130–142, http://dx.doi.org/10.1016/j.jweia.2013.09.015

[3] C J Baker, T. Johnson, D. Flynn, H. Hemida, A. Quinn, D. Soper, M. Sterling (2019) "Train Aerodynamics: Fundamentals and Applications", Elsevier

2. Outline of the analysis

In the rest of this report, we consider step by step, the chain of effects and processes that result from unsteady cross winds impinging on trains. This will be primarily through the consideration of two specific cases for a typical leading vehicle of a typical passenger train as follows.

- Case 1 for a vehicle speed of 40 m/s and a mean crosswind speed of 20m/s (the same as in Baker, 2010).
- Case 2 for the same vehicle speed and a crosswind speed of 32.5 m/s, which is near the critical wheel unloading condition.

We firstly consider the simulation of unsteady wind speeds as seen by moving vehicles in section 3, and then in section 4 show how these wind speeds produce time histories of unsteady aerodynamic forces and moments, including allowing for the non-correlation of turbulence eddies over the train surface. In section 5 we set out the calculation methodology for calculating time histories of track roughness and misalignment. Both unsteady wind loads, and track roughness effects are then used in a simple dynamic model of a train in section 6. This allows time histories of wheel unloading, track forces and vehicle displacements to be calculated. A rigorous statistical methodology is then applied to give robust maximum values of these quantities, with defined levels of probability (sections 7 to 9). A consideration of these values in section 10 leads to conclusions concerning the relative importance of a range of modelled effects.

In section 11 we then consider further the methodology for deriving cross wind characteristics in the light of the dynamic analysis and find that the results strongly suggest that the simple CWC methodology is more than adequate for practical purposes, and the complex dynamic effects are very much second order and can easily be allowed for. A fuller calibration of the CWC methodology using the dynamic model is set out in section 12 and a final discussion in section 13 addresses ways in which the methodology may be used in practice and further possible extensions are outlined.

3. Simulation of wind conditions

The first stage of the modelling process is to model the wind conditions, as experienced by the vehicle. As the starting point for this, we utilize the wind spectrum relative to a moving vehicle as set out by Cooper[4].

$$\frac{nS_u(n)}{\sigma_u^2} = \frac{4\left(\frac{nL_u}{\bar{V}}\right)}{\left(1+70.8\left(\frac{nL_u}{\bar{V}}\right)^2\right)^{5/6}}\left(\left(\frac{\bar{u}}{\bar{V}}\right)^2 + \left(1-\left(\frac{\bar{u}}{\bar{V}}\right)^2\right)\frac{\left(0.5+94.3\left(\frac{nL_u}{\bar{V}}\right)^2\right)}{\left(1+70.8\left(\frac{nL_u}{\bar{V}}\right)^2\right)}\right) \quad (3.1)$$

where n is frequency, $S_u(n)$ is the wind spectral density at a frequency n, σ_u^2 is the variance of the fluctuating wind speed,$\bar{u}$ is the mean wind speed, $\bar{V}$is the mean wind speed relative to the vehicle, and L_u is an effective turbulence length scale given by

$$L_u = L_{xu}\left(\left(\frac{\bar{u}}{\bar{V}}\right)^2 + 0.706\left(1-\left(\frac{\bar{u}}{\bar{V}}\right)^2\right)\right)^{0.5} \quad (3.2)$$

and L_{xu} is the actual wind turbulence length scale. In all the calculations that follow we assume L_{xu} = 50m and the turbulence intensity $\sigma_u/\bar{u}$ = 0.15. The spectrum of equation (3.1) is plotted in Figure 3.1 below. In effect the movement of the vehicle pushes the wind spectrum to higher frequencies than for the spectrum at a stationary point. Note that the formulation of equation (3.1) is for wind normal to the direction of travel, and this condition will be assumed in all that follows. This implies the following relationship between wind speed and vehicle speed v.

$$\bar{V}^2 = v^2 + \bar{u}^2 \quad (3.3)$$

The values of the spectral density at discrete frequencies n_j are then used to calculate the unsteady wind velocity time u_i series at time *i* at the position of the train through the following algorithm.

$$u_i = \sum_j \left(2S_u(n_j)\Delta n_j\right)^{0.5} sin\left(2\pi n_j t + 2\pi r_{ij}\right) \quad (3.4)$$

where r_{ij} is a random number between 0 and 1. The process was checked by calculating the average spectrum of 50 calculated time series. This is also shown in figure 3.1 and can be seen to be a respectable approximation to the target spectrum.

For each of the calculations that follow, two sets of 50 one-minute-long time series of velocity are calculated. These were correlated for frequencies less than 0.25 Hz (i.e. used the same random number time series) but were uncorrelated at higher frequencies. One set was used for calculating side forces and one for calculating lift forces, in an attempt to model the observed low frequency correlation between these forces in reality, but the lack of high frequency correlation.

Typical one-minute fluctuating velocity time histories for Case 1 are shown in Figure 3.2a (those for Case 2 are very similar in form, but with a greater magnitude). Figure 3.2b shows the same fluctuations over a 10 second period, where the two sets can be distinguished and can be seen to differ at the higher frequencies as expected.

[4] Cooper, R.K., 1985. Atmospheric turbulence with respect to moving ground vehicles. Journal of Wind Engineering and Industrial Aerodynamics 17, 215–238

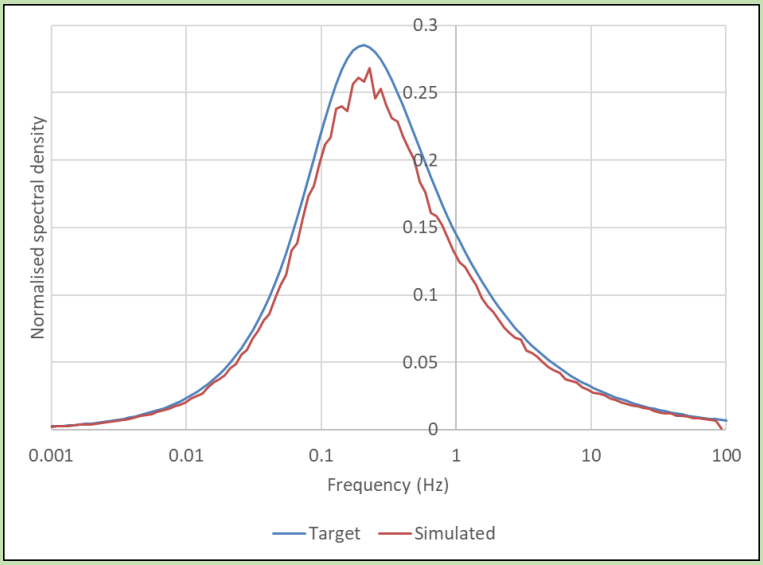

Figure 3.1 Target and simulated winds spectra

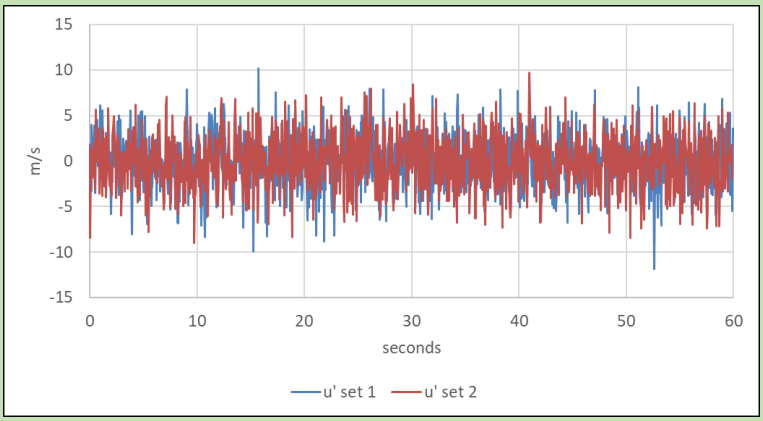

a) One minute time series

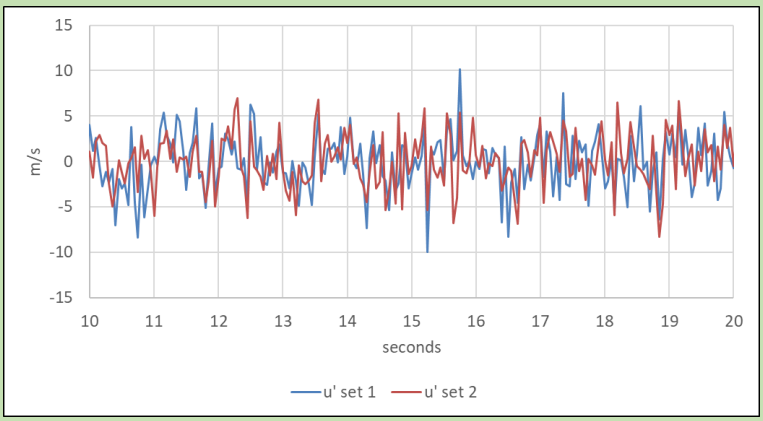

b) 10s time series

Figure 3.2. Sample simulated fluctuating wind velocity profiles for Case 1.

4. Simulation of aerodynamic forces

The next step is the specification of the aerodynamic forces and moments on the train. The prerequisite to such a calculation is a knowledge of the aerodynamic force characteristics. These are conventionally taken as functions of the yaw angle ψ. For the normal wind case this is defined as follows.

$$\tan(\psi) = \frac{\overline{u}}{v} \tag{4.1}$$

Following Baker et al (2019), we adopt the following forms, which have been shown to be a good fit to experimental data.

For low yaw angles

$$C_S(\psi) = C_S(30)\left(\frac{\sin(\psi)}{\sin(30)}\right)^{n_{S1}} \tag{4.2}$$

$$C_L(\psi) = C_L(30)\left(\frac{\sin(\psi)}{\sin(30)}\right)^{n_{L1}} \tag{4.3}$$

And for high yaw angles

$$C_S(\psi) = C_S(90)\left(\frac{\sin(\psi)}{\sin(30)}\right)^{n_{S2}} \tag{4.4}$$

$$C_L(\psi) = C_L(90)\left(\frac{\sin(\psi)}{\sin(30)}\right)^{n_{L2}} \tag{4.5}$$

The parameter values that are used are given in Table 4.1 below. These are very typical of a leading vehicle for a reasonably well streamlined train.

Table 4.1 Force coefficient parameters

$C_S(30)$	$C_S(90)$	$C_L(30)$	$C_L(90)$	n_{S1}	n_{S2}	n_{L1}	n_{L2}
4.0	5.6	2.0	2.8	1.5	1.5	-1.5	-1.5

Figure 4.1 shows a plot of the characteristics that were used.

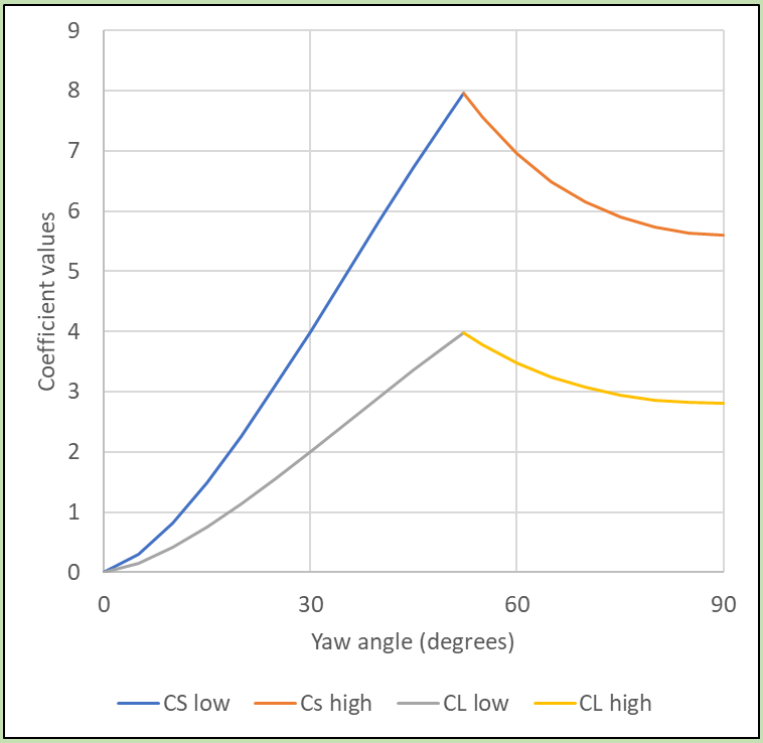

Figure 4.1. Side and lift force coefficients

The mean side and lift forces can then be calculated in the normal way from the force coefficients and the velocity relative to the train.

$$\bar{S} = 0.5\rho A\bar{V}^2 C_S \tag{4.6}$$

$$\bar{L} = 0.5\rho A\bar{V}^2 C_L \tag{4.7}$$

where ρ is the density of air (=1.22kg/m^3) and A is the train reference area (10m^2). The calculation of fluctuating forces is somewhat more complex. We use the following formulation as in Baker (2010).

$$S' = \rho A C_S \bar{u}\left(1 + \frac{1}{2C_S}\frac{dC_S}{d\psi}\cot(\psi)\right)\int_0^\infty h_S(\tau)u'(t-\tau)d\tau \tag{4.8}$$

$$L' = \rho A C_L \bar{u}\left(1 + \frac{1}{2C_L}\frac{dC_L}{d\psi}\cot(\psi)\right)\int_0^\infty h_L(\tau)u'(t-\tau)d\tau \tag{4.9}$$

$h_S(\tau)$ and $h_L(\tau)$ are the aerodynamic weighting functions for side fore and lift force respectively and allow for the filtering effect caused by the lack of correlation of forces over the train structure at higher frequencies (smaller turbulence scales). These can be obtained from wind tunnel measurements of aerodynamic admittance. The following forms are assumed in what follows.

$$h_S = (2\pi n m_S)^2 \tau e^{-2\pi n m_S \tau} \tag{4.10}$$

$$h_L = (2\pi m_L)^2 \tau e^{-2\pi m_L \tau} \tag{4.11}$$

and

$$\frac{m_S l}{\bar{V}} = 2.0\sin(\psi) \tag{4.12}$$

$$\frac{m_L l}{\bar{V}} = 2.5\sin(\psi) \qquad (4.13)$$

Here l is the train vehicle length, taken as 20m. The forms of these functions are shown in Figure 4.2. Essentially their use gives a weighted average of the instantaneous velocity over the previous 0.5s, and thus effectively act as a low pass filter.

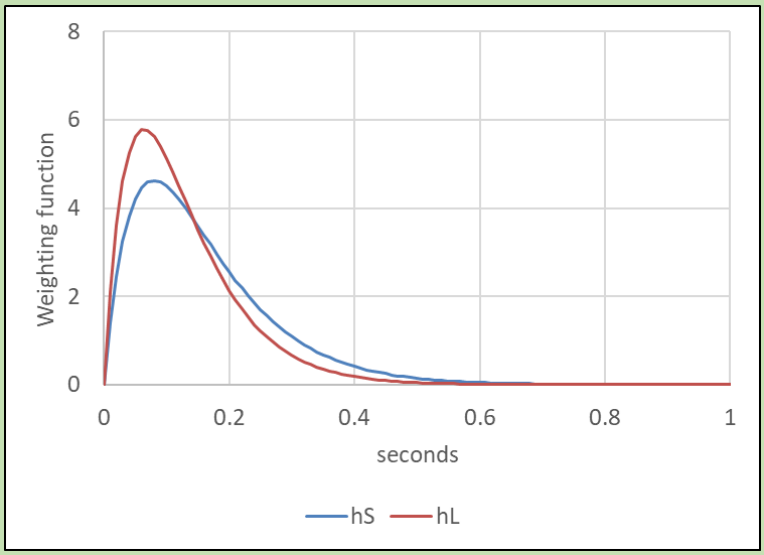

Figure 4.2. Weighting functions for side and lift force.

The overall side and lift forces are then given by the sum of the mean and fluctuating values

$$S = \bar{S} + S' \qquad (4.14)$$

$$L = \bar{L} + L' \qquad (4.15)$$

Typical one-minute realizations of side and lift forces are shown in Figure 4.3a and b for Cases 1 and 2 respectively. The effect of applying the weighting function is shown in Figure 4.4 for the side and lift forces of Case 1. In this figure, the values shown in Figure 4.3 are compared with the quasi-steady values (i.e. assuming the weighting function integrals in equations 4.8 and 4.9 have values of unity. Ten second segments are shown. The filtering effect of the weighting function is very obvious with the high frequency variations of the quasi-steady forces being damped out.

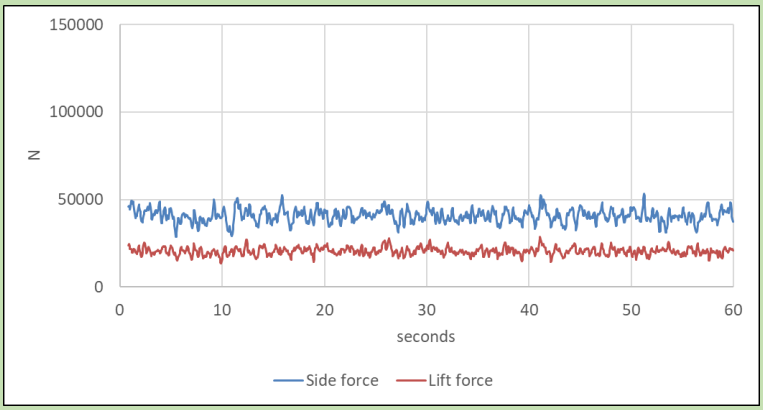

a) Case 1

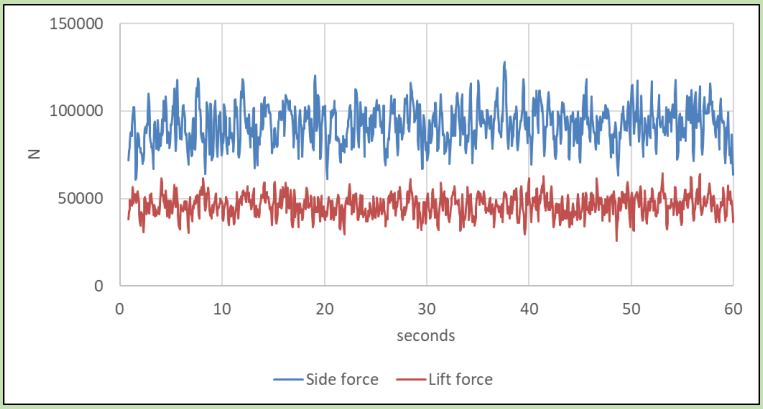

b) Case 2

Figure 4.3 Typical realisations of side and lift forces.

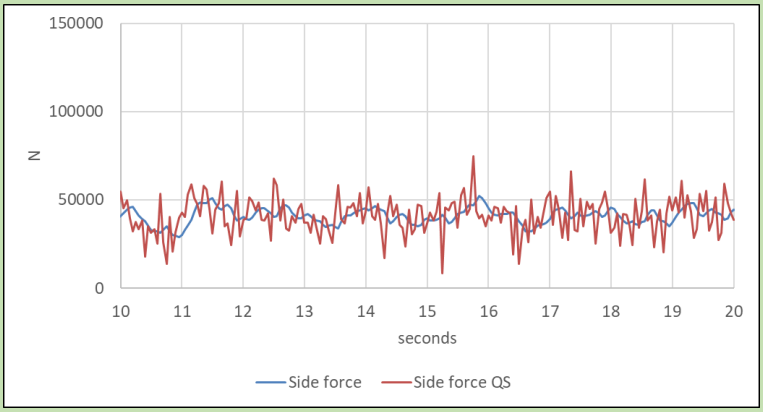

a) Side force

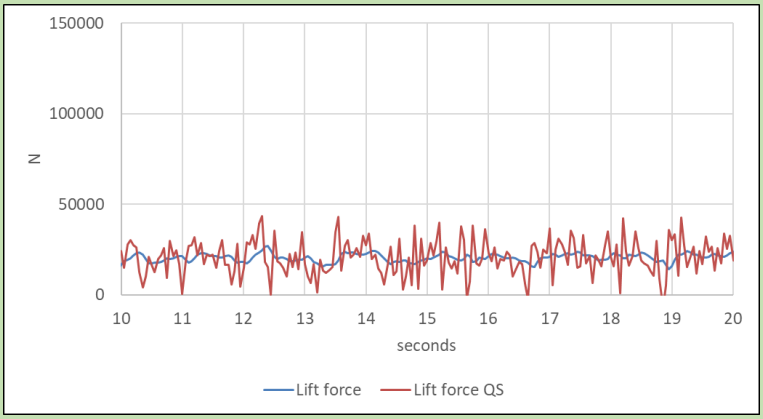

b) Lift force

Figure 4.4. Effect of application of weighting functions

Finally, it will be seen that at some points in what follows, the calculation requires the value of the lee rail rolling moment coefficient. We calculate this directly from the side and lift force coefficients as follows.

$$C_{RL} = C_S\left(\frac{q}{h}\right) + C_L\left(\frac{p}{h}\right) \qquad (4.16)$$

where q is the height of the centre of pressure above the leeward rail (taken somewhat arbitrarily as 2m), p is the track semi-width (0.75m) and h is the reference height (3m).

5. Track roughness

The track roughness is specified using the formulation of Li et al [5], which was the German high speed rail formulation of roughness. The along track alignment spectrum (in our terms the lateral roughness), the vertical profile irregularity spectrum (vertical roughness) and cross level irregularity (cross track roughness) are given by the following expressions.

$$S_x(\omega) = \frac{A_x {\omega_c}^2}{(\omega^2+{\omega_r}^2)(\omega^2+{\omega_c}^2)} \quad (5.1)$$

$$S_y(\omega) = \frac{A_y {\omega_c}^2}{(\omega^2+{\omega_r}^2)(\omega^2+{\omega_c}^2)} \quad (5.2)$$

$$S_\varphi(\omega) = \frac{(A_v/p^2){\omega_c}^2\omega^2}{(\omega^2+{\omega_r}^2)(\omega^2+{\omega_s}^2)(\omega^2+{\omega_c}^2)} \quad (5.3)$$

ω is a wavenumber and the spectral parameters are given by A_x=2.19x10^{-7} mrad, A_y= 4.032x10^{-7} mrad, ω_c= 0.8246rad/m, ω_r= 0.0206rad/m and ω_s= 0.4380rad/m. These are shown in Figure 5.1 in normalized form (i.e. spectral density x wave number / variance). The lateral and vertical spectra are identical in this format. The cross-track spectrum is different however, with the lower wave number spectral densities being much smaller.

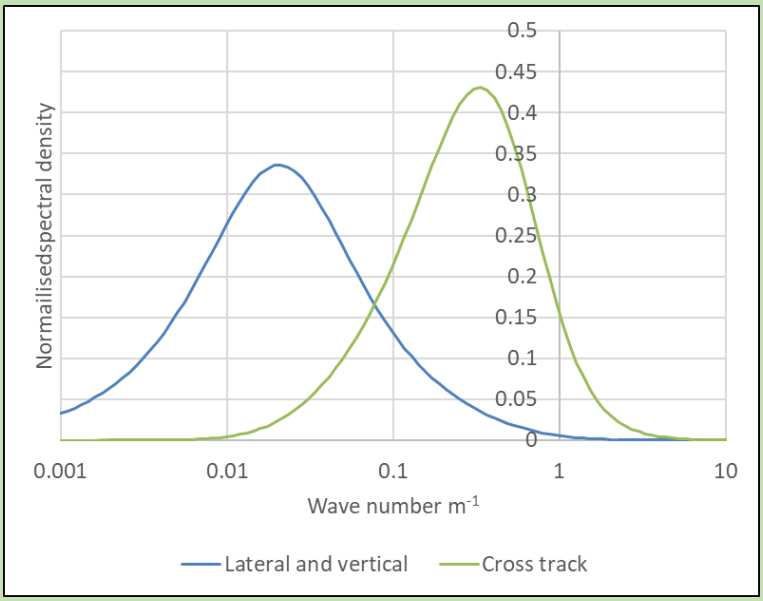

Figure 5.1 Roughness spectra

From these spectra the time history of track roughness can be obtained in a similar way to the velocity time histories

$$x_{ri} = \sum\left(2S_x(\omega_j)\Delta\omega_j\right)^{0.5} sin(\omega_j t + 2\pi r_{ij}) \quad (5.4)$$

$$y_{ri} = \sum\left(2S_y(\omega_j)\Delta\omega_j\right)^{0.5} sin(\omega_j t + 2\pi r_{ij}) \quad (5.5)$$

$$\varphi_{ri} = \sum\left(2S_\varphi(\omega_j)\Delta\omega_j\right)^{0.5} sin(\omega_j t + 2\pi r_{ij}) \quad (5.6)$$

[5] Li Y, Qiang S, Liao H, Xu Y L (2005) "Dynamics of wind–rail vehicle–bridge systems", Journal of Wind Engineering and Industrial Aerodynamics 93, 483-90 http://dx.doi.org/10.1016/j.jweia.2005.04.001

x_{ri}, y_{ri} and z_{ri} are the lateral, vertical and cross track roughness. A one-minute realization for case 1 is shown in Figure 5.2a, together with a 10s section in Figure 5.2b. It is clear that the cross-track roughness is much smaller than the lateral and vertical components. Note that as the vehicle speed is 40m/s, then the 10 second segment corresponds to a distance of 400m.

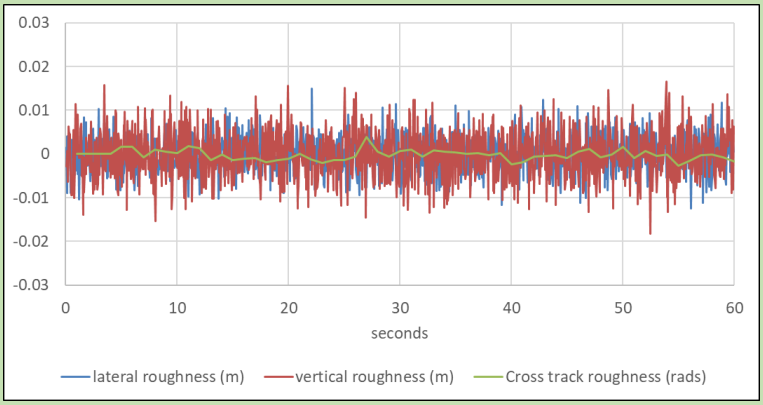

a) 60 s time history

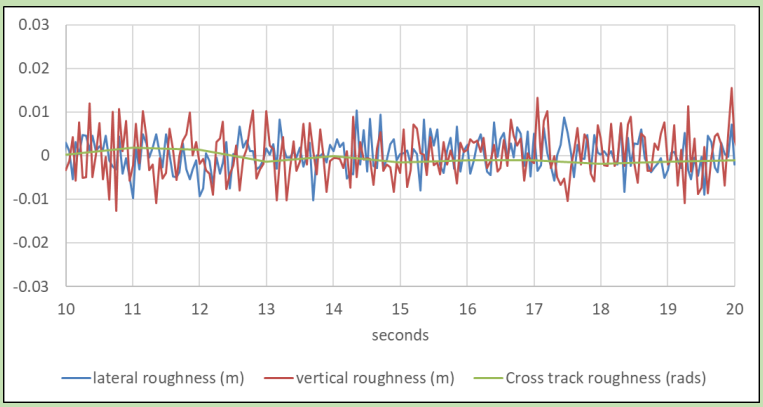

b) 10s time history

Figure 5.2 Roughness time histories for case 1 (vehicle speed 40 m/s)

6. The train suspension system under crosswind conditions

The next stage of the calculation is to apply the aerodynamic forces to some model of the vehicle system. In what follows, we use a simple three mass model – the unsprung mass (wheelsets), the primary suspended mass (bogies) and the secondary suspended mass (car body). The side and lift forces are taken to act on the car body only, and the aerodynamic forces transmitted to the rest of the vehicle through springs and dampers. There are assumed to be no interactions between lateral, vertical and rotational systems, which is of course a significant approximation. We also assume that yaw and pitch effects are not significant.

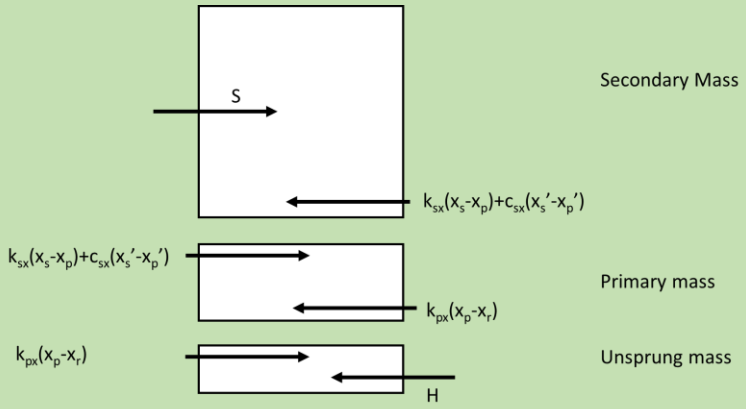

Figure 6.1 Lateral suspension system

For the lateral forces and displacements, the dynamic system is shown in Figure 6.1. We can write Newton's Law as follows for each of the three masses, which can be solved by simple numerical procedures.

Secondary mass

$$M_s \frac{d^2 x_s}{dt^2} = S - k_{sx}(x_s - x_p) - c_{sx}\left(\frac{dx_s}{dt} - \frac{dx_p}{dt}\right) \qquad (6.1)$$

Primary mass

$$M_p \frac{d^2 x_p}{dt^2} = k_{sx}(x_s - x_p) + c_{sx}\left(\frac{dx_s}{dt} - \frac{dx_p}{dt}\right) - k_{px}(x_p - x_r) \qquad (6.2)$$

Unsprung mass

$$k_{px}(x_p - x_r) = H \qquad (6.3)$$

Here M_s and M_p are the secondary and primary suspended masses; x_s and x_p are the displacements of these masses; x_r is the track displacement due to track roughness; k_{sx} and k_{px} are the stiffnesses of the primary and secondary suspensions; c_{sx} is the secondary suspension damping and H is the lateral force on the track. The primary suspension is assumed not to be damped. H is thus the side force component as modified by suspension effects. One would expect the ratio of H and S to be, on average, equal to unity. Figure 6.2 shows that this is indeed the case, although the fluctuations about this value are very large.

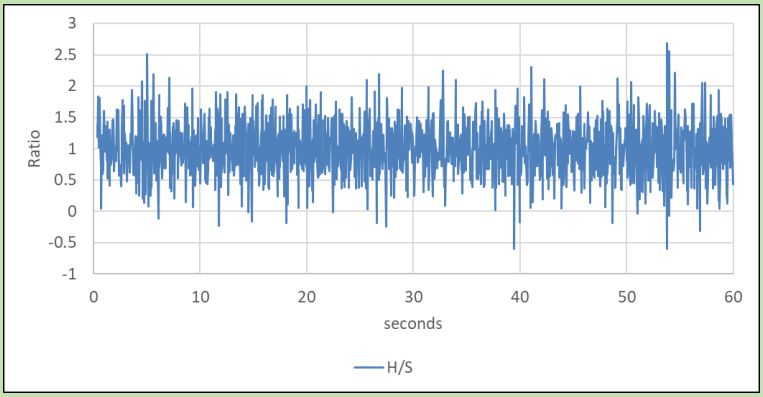

Figure 6.2 Ratio of horizontal force on track to aerodynamic side force

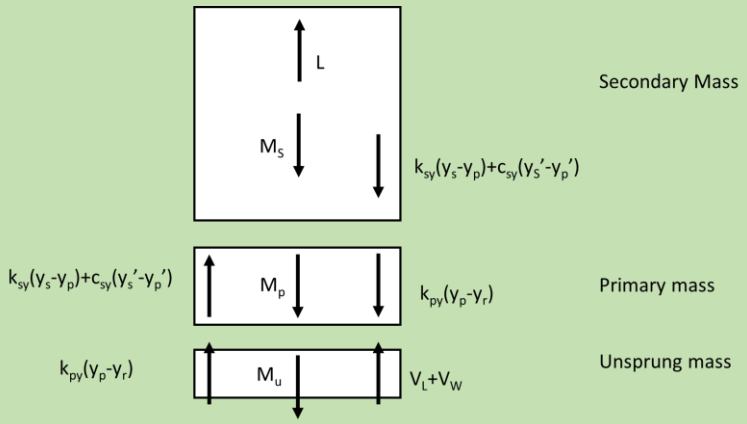

Figure 6.3 Vertical suspension system

For the vertical displacements and masses, we can write equivalent equations, with *x* replaced by *y* throughout. We do not include weight terms – these are effectively allowed for in the zero displacement conditions of the primary and secondary suspensions. The vertical dynamic system is shown in Figure 6.3 and the equations of motion are as follows.

Secondary mass

$$M_s \frac{d^2 y_s}{dt^2} = L - k_{sy}(y_s - y_p) - c_{sy}\left(\frac{dy_s}{dt} - \frac{dy_p}{dt}\right) \tag{6.4}$$

Primary mass

$$M_p \frac{d^2 y_p}{dt^2} = k_{sy}(y_s - y_p) + c_{sx}\left(\frac{dy_s}{dt} - \frac{dy_p}{dt}\right) - k_{py}(y_p - y_r) \tag{6.5}$$

Unsprung mass

$$k_{py}(y_p - y_r) + V = 0 \tag{6.6}$$

V is effectively the aerodynamic force on the track, as modified by the suspension system. One would thus again expect the ratio of this force to the lift force to be unity. Figure 6.4 shows that this is indeed the case, although, as with the *H/S* ratio, the fluctuations are very large.

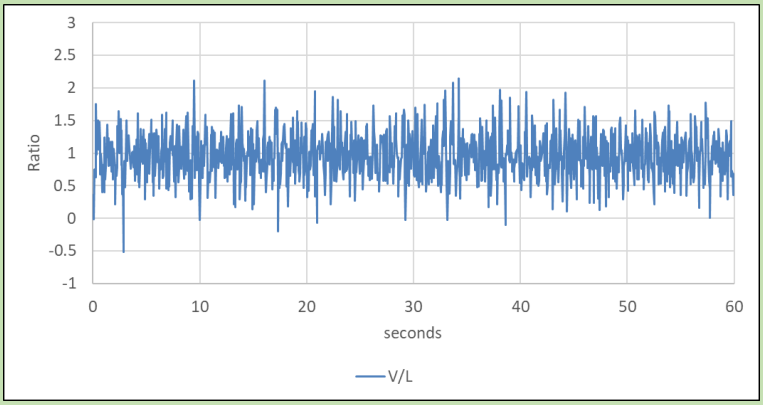

Figure 6.4 Ratio of vertical force on track to aerodynamic lift force

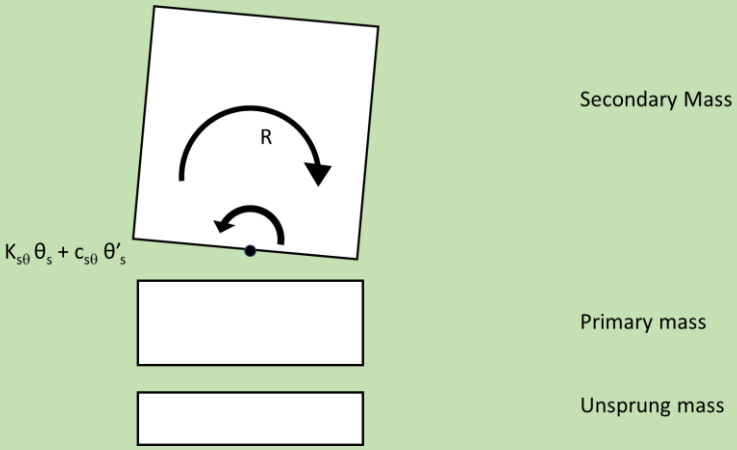

Figure 6.5 Rotational dynamic system

To model the rotational displacements, we assume that only the secondary mass rotates about a roll centre at the top of the primary mass (Figure 6.5). Using the same nomenclature as before, the equation of motion is as follows.

$$I_s \frac{d^2\theta_s}{dt^2} = R - k_{s\theta}(\theta_s - \varphi_r) - c_{s\theta}\left(\frac{d\theta_s}{dt} - \frac{d\varphi_r}{dt}\right) \qquad (6.7)$$

Here θ_s is the angle of rotation, I_s is the moment of inertia of the secondary suspended mass, and R is the rolling moment taken as

$$R = q'S \qquad (6.8)$$

where q' is the height of the centre of pressure above the roll centre.

The above equations can be easily solved through simple numerical methods. The values of the various parameters that were used are shown in Table 6.1 below, which are based upon the values given by a number or recent authors (although it has to be said there are wide variations in the values used by these authors). In solving these equations we assume that there are maximum values of primary and secondary displacements that can be allowed in the horizontal and vertical directions, and these are also given in Table 6.1.

Table 6.1 Suspension model parameters

Mass and inertia		Lateral parameters		Vertical parameters		Rotational parameters	
M_s kg	35 x 10^3	k_{sx} N/m	3 x 10^6	k_{sy} N/m	4 x 10^6	k_{sr} Nm/r	5 x 10^6
M_p kg	3 x 10^3	c_{sx} kg/s	6 x 10^4	c_{sy} kg/s	4 x 10^4	c_{sr} Nms/r	5 x 10^5
M_u kg	4 x 10^3	k_{px} N/m	1.2 X 10^7	k_{py} N/m	4 x 10^6		
I_s kg m^2	10^5	$x_{s\,max}$ m	0.04	$y_{s\,max}$ m	0.04		
		$x_{p\,max}$ m	0.01	$y_{p\,max}$ m	0.01		

The results for lateral, vertical and rotational displacement for cases 1 and 2 are shown in Figures 6.6 and 6.7 below. The difference between the two cases is basically the mean wind speed (here interpreted as a one-minute mean) – 20m/s in case 1 and 32.5m/s in case 2. This is reflected in the figures, with greater displacements in case 2 than case 1. Significantly these movements are restricted by the imposed maximum value in case 2 for the primary and secondary lateral displacements and for the primary vertical displacement.

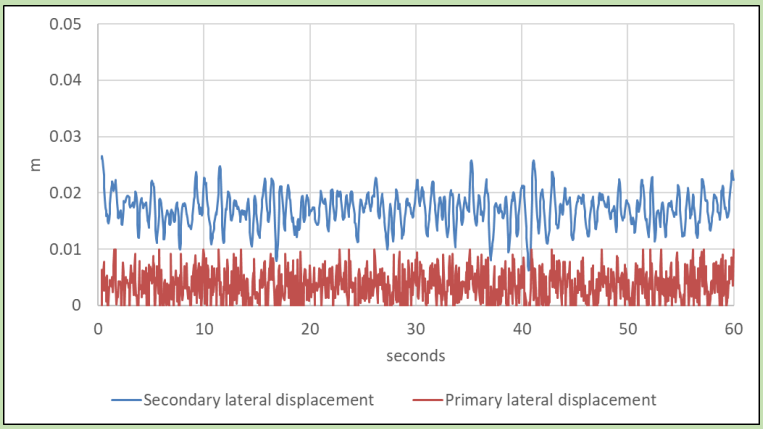

a) Lateral displacements

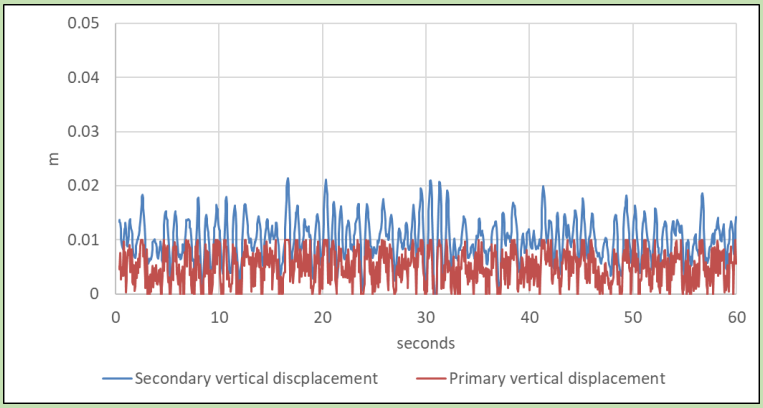

b) Vertical displacements

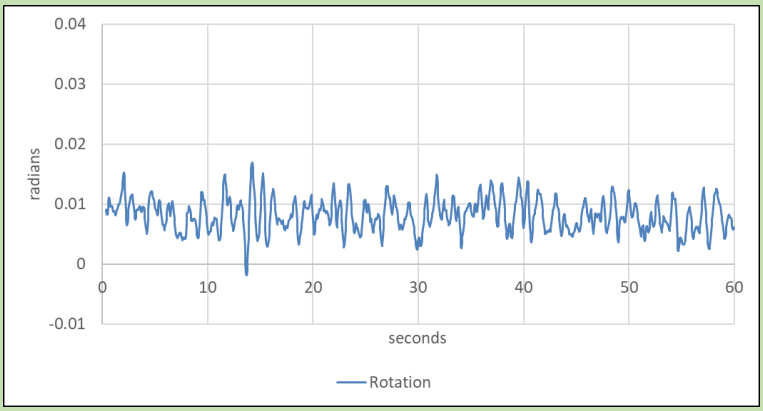

c) Rotational displacements

Figure 6.6 Calculated displacements for case 1.

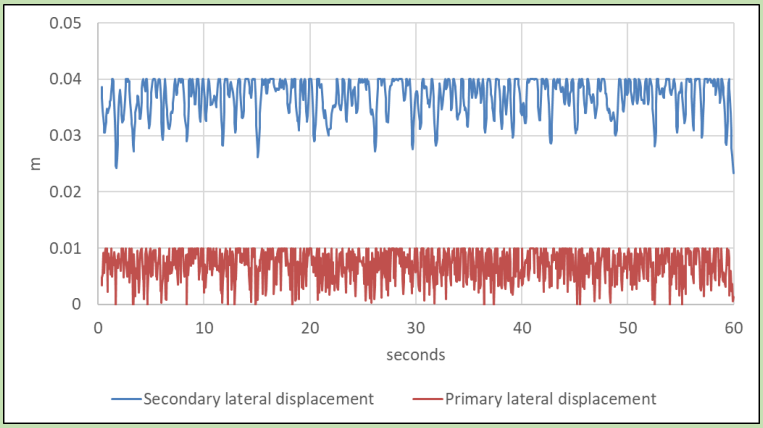

a) Lateral displacements

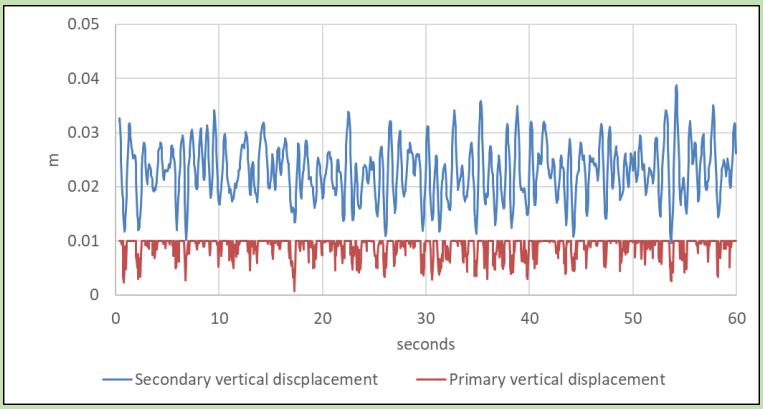

b) Vertical displacements

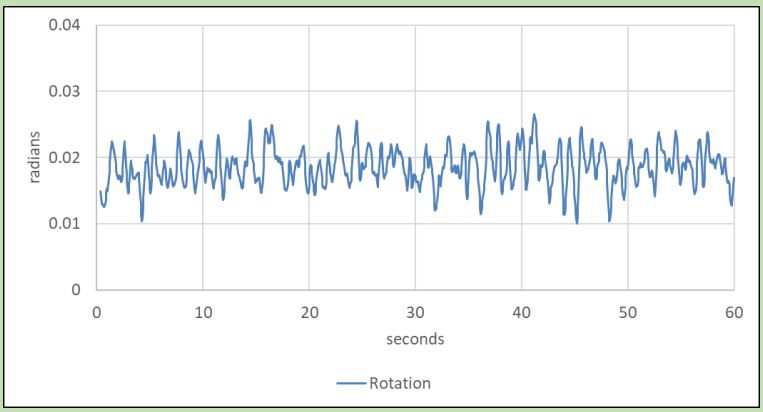

c) Rotational displacements

Figure 6.7 Calculated displacements for case 2.

7. Wheel unloading criteria

We turn now to consider the overall effects of crosswinds on trains. Perhaps the most important is the unloading of the windward wheel that in extreme cases will lead to train overturning. This unloading is the results of two moments acting about the leeward rail – the aerodynamic overturning moment, and the restoring moment due to the train masses, which may of course be displaced horizontally). The former is given by

$$R_o = Sq + Vp \tag{7.1}$$

whilst the latter is given by

$$R_r = M_u gp + M_p g(p - x_p) + M_s(p - x_s - \theta_s q') \tag{7.2}$$

The overturning and restoring moments for cases 1 and 2 are shown in Figure 7.1. For the former, the overturning moment is much less than the overturning moment, but for the latter they are much closer, with some minor crossovers.

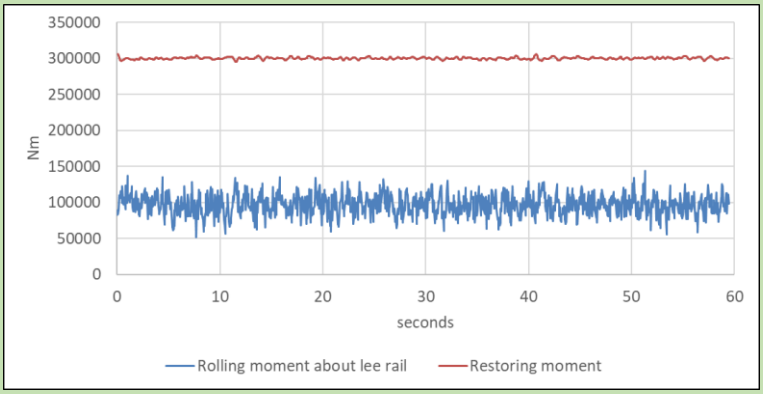

a) Case 1

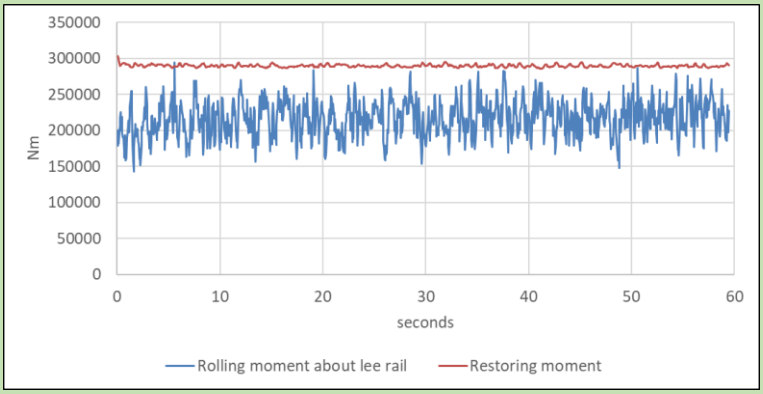

b) Case 2

Figure 7.1 Rolling and restoring moments for cases 1 and 2

By simply taking moments about the leeward rail, the windward wheel unloading is given by

$$\alpha = 1 - \frac{(R_o - R_r)}{Mgp} \tag{7.3}$$

A value of 1 indicates complete unloading. The unloadings for cases 1 and 2 are shown for one model realisation in Figure 7.2 in two forms – the instantaneous wheel unloading, and the wheel unloading with a 0.5s moving average applied, it being assumed that such a period of time is appropriate when considering whether or not dangerous conditions have been reached. It can be seen that the average unloading for case 1 is around 0.4, whilst for case 2 it averages around 0.8 with peak values close to 0.9. This value is often assumed to be the critical value for wheel unloading, and indeed the wind velocity of case 2 was chosen to achieve unloadings of this magnitude. There can be seen to be a considerable difference between the averaged and non-averaged values.

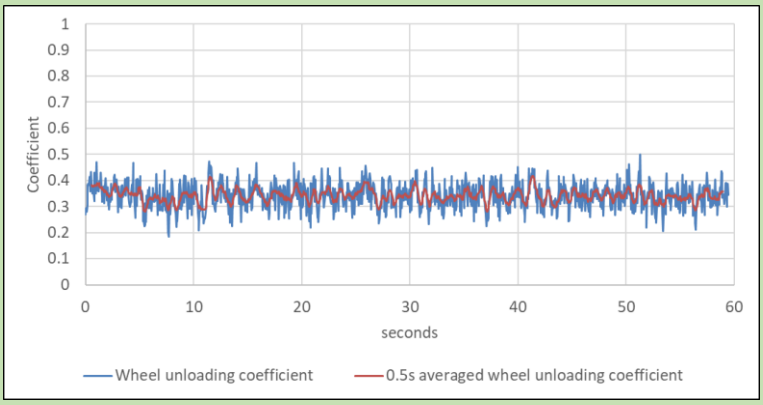

a) Case 1

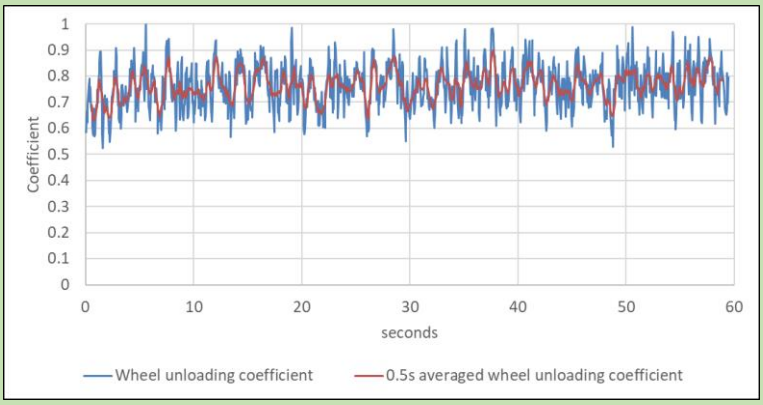

b) Case 2

Figure 7.2. Wheel unloadings for cases 1 and 2

Now, most of the figures in the preceding sections have shown the results of just a single one-minute realization of the model. Clearly there will be variability between realisations as the fluctuating forces are generated using random numbers. This is particularly important for wheel unloadings, where the peak values are important. Thus, to quantify this spread of maxima, 50 different realisations of the model were calculated. The maximum value of wheel unloading was taken for each realization $\alpha_{max,j}$ and an extreme value analysis was carried out on the ensemble of results. This assumed that the extreme values fitted a Fisher Tippet type 2 distribution of the following form.

$$1 - P_j = e^{-e^{-\frac{m_\alpha - \alpha_{max,j}}{d_\alpha}}} \tag{7.4}$$

Here P_j is the probability that $\alpha_{max,j}$ will be exceeded in any one realization, m_α is the mode of the distribution and d_α is the dispersion of the distribution. P_j is calculated from the rank of $w_{max,j}$ in the distribution, R_j, where the largest value has rank 1, and the smallest rank 50.

$$P_j = R_j/(N+1) \qquad (7.5)$$

N is the number of samples, in this case 50. The extreme value distribution are shown for cases 1 and 2 in Figure 7.3 below. $\alpha_{max,j}$ is plotted against the reduced variate $\ln\left(-\ln\left(1-P_j\right)\right)$, which should be a straight line if the distribution is of the assumed type.

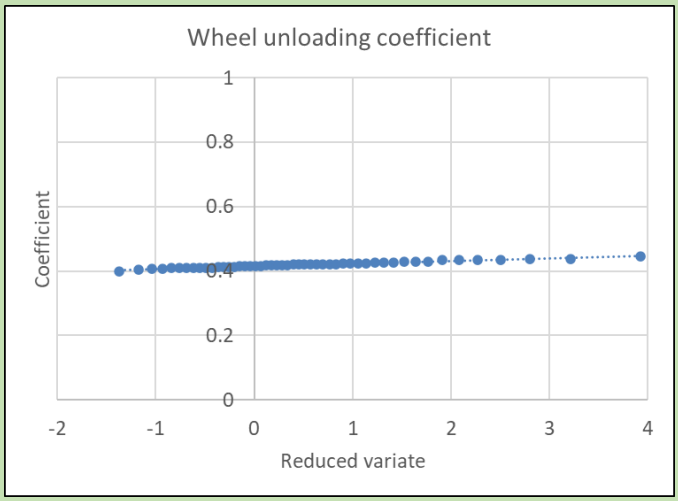

a) Case 1

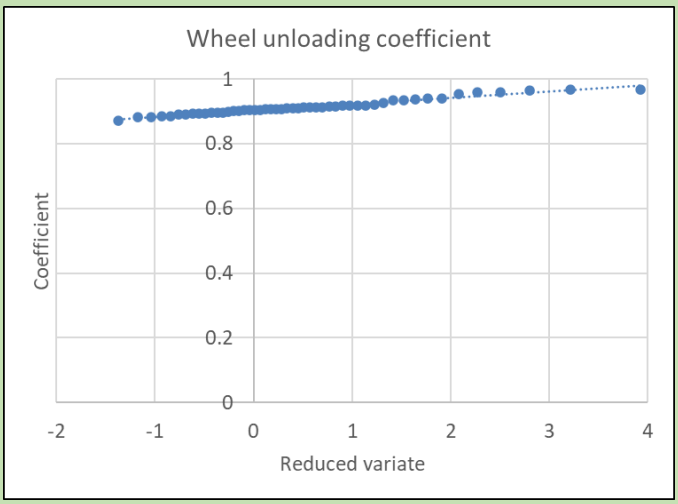

b) Case 2

Figure 7.3 Extreme value distributions for wheel unloading

In what follows we will use the mode of the distribution of wheel unloading as a robust statistical indicator of the maximum value – this is the intercept on the graphs of Figure 7.3. Note that from equation 7.4, this corresponds to a probability of exceedance of 0.632. For case 1, the mode is 0.411 and for case 2 it is 0.905, with corresponding dispersion of 0.008 and 0.019.

8. Track force criteria

Another effect of cross wind is to increase the lateral load on the windward track. The criterion that is usually applied for assessing whether or not such loads are acceptable is the Nadal criterion, which states that the ratio of the horizontal to vertical force on the leeward rail should not exceed 0.8. In the terms of this paper, this ratio is given by the following formula.

$$\mu = \frac{2S}{M_t g - L + S(q/p)} \qquad (8.1)$$

Here M_t is the overall vehicle mass. The coefficients for cases 1 and 2 are shown in Figure 8.1 below for both the raw and the 0.5 second averaged values as before. Even for the higher speed case 2, the values fall well below the limit of 0.8. An extreme value analysis was carried out in the same way as for wheel unloading which gave values of the mode m_μ of 0.185 for case 1 and 0.333 for case 2, and for the dispersion d_β of 0.003 and 0.004.

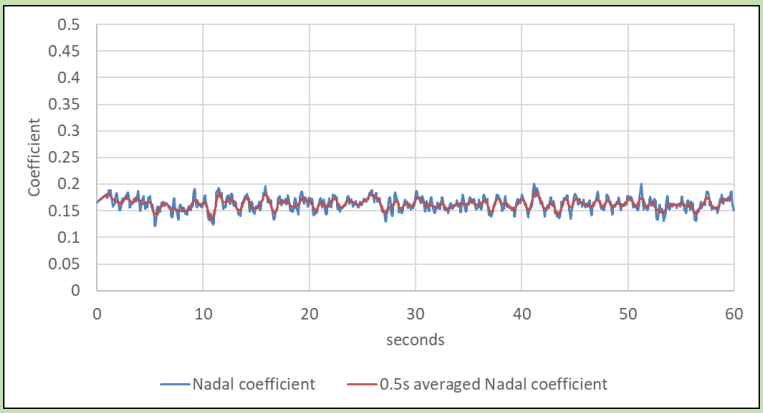

a) Case 1

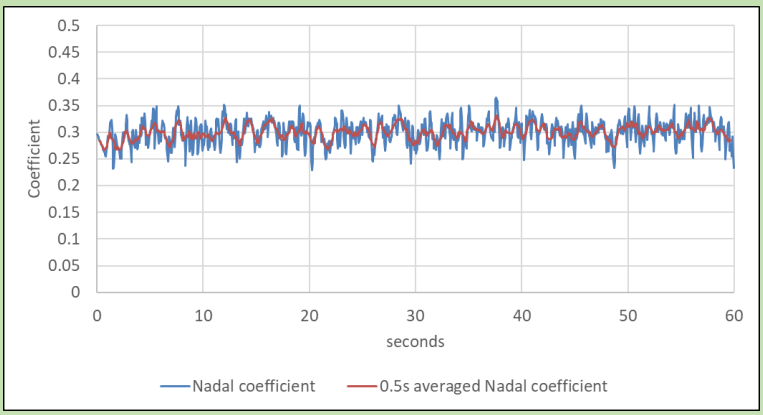

b) Case 2

Figure 8.1Time histories of Nadal coefficient

9. Roof displacement criteria

The third effect of crosswinds on trains that we consider here is the displacement of the train body, potentially leading to the infringement of the kinematic envelope, or causing dewirement of the pantograph. We quantify this by defining the following roof displacement coefficient, which is the ratio of the lateral displacement of the roof due to movement on the suspension and to roll to the vehicle reference height of 3m.

$$\gamma = \frac{\theta l + x_p + x_s}{h} \qquad (9.1)$$

Again, time histories of the coefficient can be obtained and one-minute realisations of these are shown in Figure 9.1 below. For case 1 the coefficient is around 0.015 and for case 2 around 0.03, representing lateral movements of 4.5 and 9cm respectively. We do not apply the 0.5s average in this case, as instantaneous values are of most significance i.e on very short-term exceedance causing some sort of contact with another body is the critical case.

An extreme value analysis was again carried out in the same way as for wheel unloading which gave values of the mode of 0.0224 for case 1 and 0.0388 for case 2, and for the dispersion d_β of 0.0009 and 0.0010.

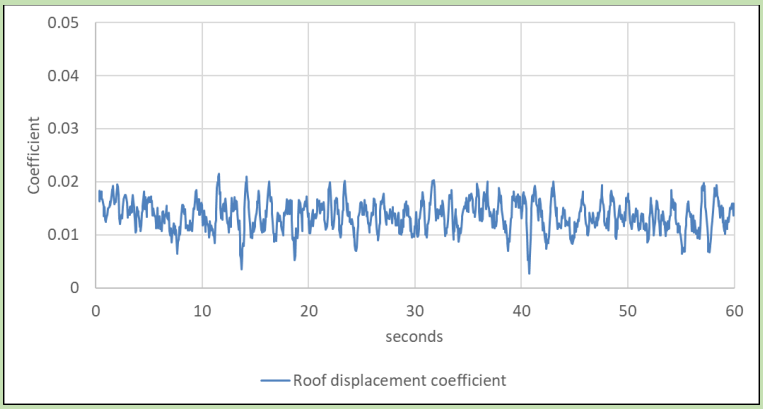

a) Case 1

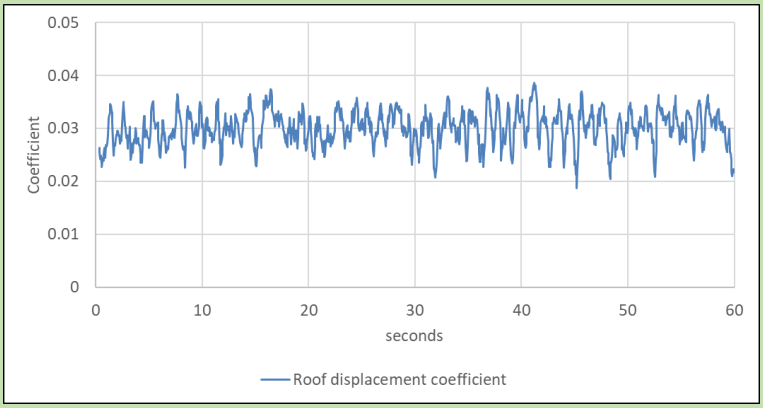

b) Case 2

Figure 9.1 Roof displacement coefficient time history

10. Parametric analysis

The methodology of extreme value analysis can be used to assess the relative magnitudes of the different effects that have been modelled. In table 10.1 we present data for the modes of the coefficients α, μ and γ for cases 1 and 2 for the following cases.

- With no suspension, roughness or admittance effects modelled i.e. the simple QS steady three mass case with no movement on the suspension.
- Each of suspension, roughness or admittance (weighting function) effects added singly to the QS case.
- The three effects added in pairs to the QS case.
- All three effects included (the results from sections 7, 8 and 9).

An examination of the results in the Table 10.1 shows the following.

- The effects of roughness are very small throughout, changing the mode values by less than 0.01 in most cases, the exception being the roof displacement criteria, where the short-term fluctuations are not eliminated by the taking of the 0.5s s average. The inclusion of roughness usually (but not always) increases the mode, making the effect more noticeable.
- The effects of admittance are generally to reduce the modes by around 0.02. This is again due to the filtering out of the short-term peaks.
- The effect of including suspension effects (lateral movement and roil) is to increase the modes by around 0.03.

Thus, it can be seen that suspension effects are the most significant, but even here the change to the QS values are not very large. It will be seen in what follows that this has practical implications.

Table 10.1 Modes for Cases 1 and 2, for different calculation types

		Case 1 v= 40m/s u = 20m/s			Case 2 v= 40m/s u = 32.5m/s		
Line	Case	m_α	m_μ	m_γ	m_α	m_μ	m_γ
1	QS only	0.385	0.189	0	0.865	0.337	0
2	QS + admittance	0.370	0.186	0	0.832	0.336	0
3	QS + roughness	0.384	0.189	0	0.864	0.335	0
4	QS + admittance + roughness	0.369	0.185	0	0.840	0.333	0
5	QS + suspension	0.419	0.189	0.0188	0.927	0.336	0.0363
6	QS + admittance + suspension	0.405	0.185	0.0178	0.903	0.333	0.0357
7	QS + roughness + suspension	0.425	0.189	0.0231	0.927	0.336	0.0392
8	QS + admittance + roughness + suspension	0.411	0.185	0.0224	0.905	0.333	0.0388

11. Specification of cross wind characteristics

In this section we present a simple analytical approach to the study of crosswind effects on trains and use the analysis of the preceding sections to calibrate and verify the adequacy of this simplified approach. We begin by considering the case of a rail vehicle in a cross wind going through a curve of curvature C on canted track with a small cant angle ε. As in section 6, we assume a three-mass vehicle, with an unsuspended (unsprung) mass of M_u (the wheelsets), a primary suspended mass of M_p (the bogie frames) and a secondary suspended mass of M_s (the train body). The total mass is M_t. The track semi-width is *p*, and the centre of gravity heights of the unsprung, primary, secondary and total masses above the rail are s_u, s_p, s_s and s_t respectively. The wind is assumed to blow from the centre of the curve, displacing the centre of gravity of primary and secondary masses by distances x_p and x_s laterally, and the distance of the overall centre of gravity by a distance x_t laterally. The wheel unloading is α.

The moments tending to overturn the vehicle are the aerodynamic rolling moment about the leeward rail and the moment due to centrifugal force.

$$R_o = C_{RL}(0.5\rho AhV^2) + (M_t C s_t v^2 \cos(\varepsilon) - M_t C(p - x_t)v^2 \sin(\varepsilon)) \quad (11.1)$$

The restoring moment is provided by the displaced masses.

$$R_r = M_u gp\cos(\varepsilon) + M_p g(p - x_p)\cos(\varepsilon) + M_s g(p - x_s)\cos(\varepsilon) + M_u g s_u \sin(\varepsilon) + M_p g s_p \sin(\varepsilon) + M_s g s_s \sin(\varepsilon) \quad (11.2)$$

The difference between these two moments is the moment caused by the reduced force on the windward wheel $M_t gp(1-\alpha)$. Thus we can write

$$M_t gp(1-\alpha) + C_{RL}(0.5\rho AhV^2) + M_t C s_t v^2 \cos(\varepsilon) - M_t C(p - x_t)v^2 \sin(\varepsilon) = M_u gp\cos(\varepsilon) + M_p g(p - x_p)\cos(\varepsilon) + M_s g(p - x_s)\cos(\varepsilon) + M_u g s_u \sin(\varepsilon) + M_p g s_p \sin(\varepsilon) + M_s g s_s \sin(\varepsilon) \quad (11.3)$$

Now if there were no cross winds, and the curvature forces were balanced by the lateral forces on the track, we can define the balancing speed v_b through the following expression.

$$M_t g \sin(\varepsilon) = M_t C {v_b}^2 \cos(\varepsilon) \quad (11.4)$$

From equations 11.3 and 11.4 and making the assumption that the cant angle is small, one obtains the following expression.

$$C_{RL}(0.5\rho AhV^2) = M_t gp\left(\alpha - \frac{M_s x_s}{M_t p} - \frac{M_p x_p}{M_t p} + \frac{C s_t (v_b^2 - v^2)}{gp}\right) \quad (11.5)$$

We now assume that the displacement of the primary suspended mass x_p is the distance to the primary bump stop $x_{p\,max}$. The displacement of the secondary suspended mass has two components - one due to lateral displacement and one due to rotational displacement. We can assume that the former is given by the distance to the secondary bump stop and can thus write.

$$x_s = x_{s\,max} + x_{s\,rot} \tag{11.6}$$

$x_{s\,rot}$ is assumed to be given by

$$x_{s\,rot} = C_R(0.5\rho AhV^2)\frac{s_s'}{k_{s\theta}} \tag{11.7}$$

Here C_R is the rolling moment coefficient about the roll centre, and s_s' is the distance of the centre of gravity of the secondary mass to the roll centre; $k_{s\theta}$ is the rotational stiffness in Nm/rad and can be expressed as $k_{s\theta} = M_{sp}gs_t(1+s)/s$ where s is the suspension coefficient. Thus $x_{s\,rot}$ is given by

$$x_{s\,rot} = C_R(0.5\rho AhV^2)\frac{s_s'}{s_t}\frac{s}{M_{sp}g(1+s)} \tag{11.8}$$

Now we assume

$$\epsilon = \frac{s_s'}{s_t}\frac{C_R}{C_{RL}} \tag{11.9}$$

and thus

$$x_{s\,rot} = C_{RL}(0.5\rho AhV^2)\epsilon\frac{s}{M_{sp}g(1+s)} \tag{11.10}$$

It can be shown that ϵ has a value of around 0.3, although it will be seen the precise value is not critical. After some manipulation equation 11.5 can be written as follows.

$$C_{RL}(0.5\rho AhV^2) = M_t gp\left(\frac{1+s}{1+(1+\epsilon)s}\right)\left(\alpha - \frac{M_s x_{s\,max}}{M_t p} - \frac{M_p x_{p\,max}}{M_t p} + \frac{Cs_t(v_b^2 - v^2)}{gp}\right) \tag{11.11}$$

Now since ϵ is of the order of 0.3, and s takes values of around 0.1 to 0.2, and as both are small, we can expand the first term in brackets on the right-hand side of the equation as follows.

$$C_{RL}(0.5\rho AhV^2) = M_t gp(1-\epsilon s)\left(\alpha - \frac{M_s x_{s\,max}}{M_t p} - \frac{M_p x_{p\,max}}{M_t p} + \frac{Cs_t(v_b^2 - v^2)}{gp}\right) \tag{11.12}$$

We write this as

$$C_{RL}(0.5\rho AhV^2) = M_t gp(f_{s1})(\alpha - f_{s2} + f_c) \tag{11.13}$$

$$f_{s1} = (1-\epsilon s) \tag{11.14}$$

$$f_{s2} = \left(\frac{M_s x_{s\,max}}{M_t p} + \frac{M_p x_{p\,max}}{M_t p}\right) \tag{11.15}$$

$$f_c = \left(\left(\frac{v_b}{v}\right)^2 - 1\right)\frac{qCv^2}{pg} \tag{11.16}$$

where the parameters f_{s1}, f_{s2} and f_c represent rotational suspension effects, lateral suspension effects and curvature effects respectively. By analogy one can then also include other suspension effects, admittance effects and track roughness effects in a similar way.

$$C_{RL}(0.5\rho AhV^2) = Mgp(f_{s1})(\alpha - f_{s2} - f_{s3} - f_a - f_r + f_c) = Mgp\alpha' \quad (11.17)$$

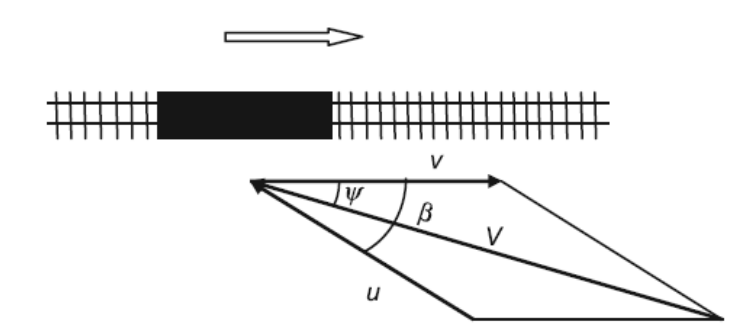

Figure 11.1 Velocity vectors

Now consider the generalized velocity diagram for a train shown in Figure 11.1. From this figure one can write

$$V^2 = ((ucos(\beta) + v)^2 + (usin(\beta))^2) \quad (11.18)$$

$$\tan(\psi) = \frac{u \sin(\beta)}{u\, cos(\beta)+v} \quad \text{or} \quad \sin(\psi) = \frac{u \sin(\beta)}{((u\, cos(\beta)+v)^2+(u \sin(\beta))^2)^{0.5}} \quad (11.19)$$

Now for the lee rail rolling moment coefficient low yaw angles we can write (as for side and lift force coefficient in equations 4.2 to 4.5)

$$\frac{C_{RL}(\psi)}{C_{RL}(30)} = \left(\frac{\sin(\psi)}{\sin(30)}\right)^{n_{R1}} \quad (11.20)$$

And at high yaw angles

$$\frac{C_{RL}(\psi)}{C_{RL}(90)} = \left(\frac{\sin(\psi)}{\sin(90)}\right)^{n_{R2}} \quad (11.21)$$

From equations 11.17 to 11.20 we can write, after some manipulation

$$c^2 = \frac{\alpha' Mgp\,(\sin(30))^{n_{R1}}}{0.5\rho C_{RL}(30)Ah} = V^2(\sin(\psi))^n = (v^2 + {u_o}^2 + 2u_o v cos(\beta))^{(2-n_{R1})/2} {u_o}^{n_{R1}} (\sin(\beta))^{n_{R1}} \quad (11.22)$$

where u_o is the wind gust velocity at which the wheel unloading reaches a specific value α. We define c as a characteristic velocity and use it as a normalisation velocity. This gives the following cross wind characteristic (CWC) at low yaw angles.

$$\left(\bar{v}^2 + {\bar{u}_o}^2 + 2\bar{u}_o\bar{v}cos(\beta)\right) = (\bar{u}_o \sin(\beta))^{2n_{R1}/(n_{R1}-2)} \quad (11.23)$$

Here the overbar denotes normalization with c. Similarly at high yaw angles one obtains

$$\left(\bar{v}^2 + {\bar{u}_o}^2 + 2\bar{u}_o\bar{v}cos(\beta)\right) = \left(\frac{2^{n_{R1}}}{C_{RL}(90)/C_{RL}(30)}\right)^{2/(n_{R1}-2)} (\bar{u}_o \sin(\beta))^{2n_{R1}/(n_{R1}-2)} \quad (11.24)$$

Equations 11.23c and 11.24 give relatively straightforward expressions for the CWCs that Baker (2013) are in very good agreement with those calculated using much more complex methods. However, to be useful in design, then it is necessary that the value of c be specified *a priori* from the train parameters ie using equation 11.22. This requires a knowledge of the parameter α' and thus the parameters of equation 11.17 that describe suspension, admittance, roughness and curvature effects.

In the next section we will derive the values of these parameters from the dynamic model set out in sections 3 to 10.

12. Calibration of CWC model

As noted in the last section, the CWC model developed there is only useful if the characteristic velocity can be specified a priori. This requires the specification of the various parameters that allow for suspension effects etc. In this section we determine values of these parameters, and show that the values of the characteristic velocities thus calculated are consistent with the CWCs calculated from wind gust speeds. The methodology we use is as follows.

- Use the vehicle characteristics (geometric, aerodynamic, suspension etc.) used in the earlier sections for a range of vehicle speeds between 20m/s and 60m/s.
- Using the full model, for each vehicle speed adjust the input wind speed (which are essentially one minute means), so that the mode of 50 model realisations of the wheel unloading m_α is as close to 0.9 as possible.
- In the same calculations record the equivalent mode of the wind gust velocity m_u.
- Run the same calculations at all vehicle speeds without any allowances for suspension, admittance or roughness. The values of m_α thus obtained, $m_{\alpha 0}$, are given by a highly simplified version of equation 11.17.

$$m_{\alpha 0} = \frac{C_{RL}\left(0.5\rho AhV^2\right)}{Mgp} \qquad (12.1)$$

- Repeat the same calculations with suspension roll effects included to give a further mode of the wheel unloadings, $m_{\alpha 1}$. From equations 11.17 and 12.1 the suspension roll parameter f_{s1} is given by

$$f_{s1} = \frac{m_{\alpha 0}}{m_{\alpha 1}} \qquad (12.2)$$

- Repeat the calculations, but with the sprung masses at their maximum values, to give a further set of modes at each wind speed $m_{\alpha 2}$. From equations 11.17, 12.1 and 12.2 we obtain.

$$f_{s2} = m_{\alpha 2} - m_{\alpha 1} \qquad (12.3)$$

- Continue the process by sequentially adding full suspension and roughness, to give two more sets of modes $m_{\alpha 3}$ and $m_{\alpha 4}$. From these we can obtain.

$$f_{s3} = m_{\alpha 3} - m_{\alpha 2} \qquad (124)$$

$$f_r = m_{\alpha 4} - m_{\alpha 3} \qquad (12.5)$$

- f_a can then be calculated from

$$f_r = 0.9 - m_{\alpha 4} \qquad (12.6)$$

- The equivalent value of the characteristic wind speed for each vehicle speed can then be calculated from equation 11.22.
- The parameters f_{s1} and f_{s2} can also be calculated directly from equations 11.14 and 11.15.

The results of such a calculation are shown in Table 12.1 below.

Table 12.1 Model calibration

$C_{RL}(30)$	3.17					
$C_{RL}(90)$	4.43					
n_{R1}	1.50					
n_{R2}	-1.50					
Overall mass (kg)	42000					
Primary mass (kg)	3000					
Secondary mass (kg)	35000					
Maximum movement of primary mass (m)	0.01					
Maximum movement of secondary mass (m)	0.04					
Track semi-width (m)	0.75					
Vehicle speed (m/s)	20	25	30	40	50	60
Wind speed (m/s)	44.6	39.8	33.7	32.5	31.2	32.1
Wheel unloading	0.90	0.90	0.90	0.90	0.90	0.90
f_{s1}	0.9756	0.9762	0.9716	0.9603	0.9685	0.9726
f_{s1} from equation 11.14	0.9700					
f_{s2}	0.0426	0.0460	0.0494	0.041	0.0414	0.0454
f_{s2} from equation 11.15	0.0454					
f_{s3}	0.0045	0.0064	0.0126	0.0167	0.0096	0.0004
f_r	-0.0059	0.0014	-0.0011	-0.0007	0.0014	0.0005
f_a	-0.0067	-0.0105	-0.0141	-0.0199	-0.0232	-0.0196
c (m/s)	40.10	39.99	39.86	39.69	40.05	40.28
c (m/s) from CWC fit	40.40					

From this table we can observe the following.

- The values of f_{s1}, the roll suspension parameter, are all slightly below 1.0, with an average value of 0.971 and a standard deviation of 0.006. The value from equation 11.14 is 0.970, well within the standard deviation range.
- The values of f_{s2}, the lateral suspension parameter have an average value of 0.044 and a standard deviation of 0.003. The value from equation 11.15 is 0.045, well within the standard deviation range.
- The value of f_{s3}, the parameter describing other suspension effects, has an average value of 0.008 and a standard deviation of 0.005.

- The value of f_r, the parameter describing roughness effects, has an average value of -0.001 and a standard deviation of 0.003.
- The value of f_a, the parameter describing admittance effects, has an average value of -0.016 and a standard deviation of 0.006.
- The calculated values of the characteristic wind speed c have an average of 40.0m/s and a standard deviation of 0.2m/s.

It can thus be seen that the parameters concerned with suspension roll and lateral movement f_{s1} and f_{s2} in the calculation of characteristic wind speed. These effects both act to destabilise the vehicle, broadly by moving the centre of gravity towards the leeward rail, and thus reducing the restoring moment. Other suspension effects, as given by f_{s2} are similar, but much smaller in magnitude. The effect of track roughness (f_r) is minimal, whilst the effect of admittance (f_a) is to stabilize the vehicle (through filtering out high frequency wind gusts, but the effect is again not large. The sum of the averages of last three of these factors is -0.008, and the combined effects can probably be ignored in comparison to the roll and lateral movement suspension effects. Both of these can of course be predicted a priori from equations 11.14 and 11.15, opening the possibility of straightforward calculations of characteristic windspeed, and thus CWCs, in vehicle design. If this is done, the characteristic wind speed is very similar to the average value at 39.8m/s.

A further comparison can be made. The modes of gust velocity at different vehicle speeds can be plotted, and a CWC fitted using equations 11.23 and 11.24, to obtain the best fit value of characteristic velocity. This is shown in Figure 12.1. The best fit value of c is 40.4 m/s – close to the values from table 12.1, but outside the standard deviation range. Nonetheless the agreement is very encouraging.

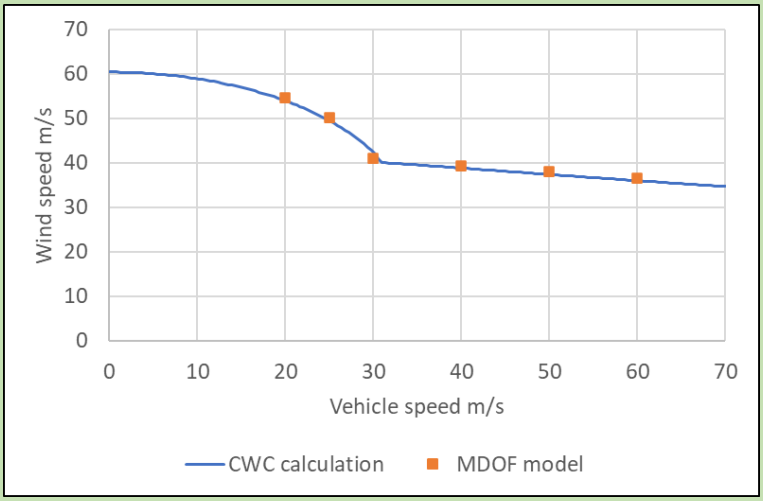

Figure 12.1 CWC curve fitted to modes of gust values

13. Discussion

13.1 Use of wheel unloading CWC methodology

The methodology for calculating wheel unloading CWCs set out in section 11 and calibrated in section 12 offers a potentially powerful design methodology. It basically requires knowledge of the lee rail rolling moment coefficient for a particular train shape (from wind tunnel tests or CFD calculations and the basic geometric and weight characteristics of the vehicle, which are used to calculate a characteristic velocity. The previous two sections have shown that only the basic suspension parameters (the suspension coefficient and the distances to the bump stops) are of any significance in the calculation. Such CWCs give the gust speed at which the train will experience a specified degree of wheel unloading. This gust speed needs careful definition however – it is the one second averaged gust speed as seen by the train i.e. over a specific length of track. This is thus both a spatially and temporally averaged gust. Nonetheless the methodology allows the CWCs to be developed quite straightforwardly during the design phase of the train from equations 11.123 and 11.24 – although a simple numerical iteration method is required.

Once such a curve has been derived, it can be used in a variety of ways.

- The method gives an indication of the overturning wind speed at different vehicle speeds, so the effects of speed restrictions can be appreciated.
- Different wheel unloading specifications can also be investigated as can potential changes to the major suspension parameters.
- Higher levels of track roughness than those used here (which were high speed track specifications) could be used to look at the effect of poor-quality track on wheel unloading in cross winds.
- The equation for characteristic wind speed also contains a curvature term, and it is a straightforward matter to modify the values of this parameter, and thus the CWCs for a variety of different track curvatures.
- The overall methodology can then be easily input into whole route risk assessment methodologies that considers the sum of risk on individual track sections.

In summary, in comparison to current methods which use MDOF train dynamic models with artificial wind gusts [6], it offers a very much simpler way of doing things, with no particular loss of accuracy.

13.2 Extensions to the methodology

The methodology outlined in section 11 can also be adapted to other cross wind effects – and in particular the development of CWCs based on limiting values of the Nadal coefficient and the roof displacement, through the definition of characteristic wind speeds for these effects. We consider these briefly in what follows.

From equation 8.1, the Nadal coefficient is given by

$$\mu = \frac{2S}{M_t g - L + S(q/p)} \qquad (13.1)$$

[6] CEN (2018) EN 14067-6:2018(MAIN) Railway applications - Aerodynamics - Part 6: Requirements and test procedures for cross wind assessment

Using the formulations for side and lift force coefficients given earlier one can obtain

$$V^2(\sin(\psi))^n = \frac{\mu Mg(\sin(30))^{n_{s1}}}{0.5\rho AC_s(30)\left(2+\mu\left(\frac{C_L}{C_S}-\frac{q}{p}\right)\right)} \quad (13.2)$$

From equation 11.22 we can thus define a characteristic wind speed for specific values of the Nadal coefficient c_μ.

$$c_\mu{}^2 = \frac{\mu Mg(\sin(30))^{n_{s1}}}{0.5\rho AC_s(30)\left(2+\mu\left(\frac{C_L}{C_S}-\frac{q}{p}\right)\right)} \quad (13.3)$$

This analysis assumes that the ratio of lift force to side force is constant, which is absolutely true for the analysis in the previous sections and is a generally good approximation in practice. The value of c_μ for Case 2, with a modal value of the Nadal coefficient of 0.333 is 39.4m/s which is close to, although a little below, the value for wheel unloading at the same conditions. The difference will be due to the dynamic effects used in the dynamic vehicle model. For the normal limit Nadal, the value of c_μ becomes 133m/s, which gives an unrealistically high CWC. On the basis that the Nadal limit seems unlikely to be exceeded in the case considered here, it is perhaps not necessary to refine the analysis further to take into account suspension effects.

If we define a limit value of roof displacement of X, we can write this as

$$X = x_{pmax} + x_{smax} + \frac{q\prime}{\sigma}(0.5\rho AV^2C_S)l = x_s + \frac{s}{1+s}\frac{q\prime}{s_t}\frac{(0.5\rho AV^2C_S)}{M_sg}l \quad (13.4)$$

From which one can obtain

$$V^2(\sin(\psi))^n = \frac{(X-x_{smax}-x_{pmax})M_sg(\sin(30))^{n_{s1}}}{0.5\rho AC_s(30)l}\frac{s_t}{q\prime}\frac{1+s}{s} \quad (13.5)$$

and a further characteristic velocity for roof displacement

$$c_X{}^2 = \frac{(X-x_{smax}-x_{pmax})M_sg(\sin(30))^{n_{s1}}}{0.5\rho AC_s(30)l}\frac{s_t}{q\prime}\frac{1+s}{s} \quad (13.6)$$

Again, substituting the parameters for Case 2, where the mode of the displacement was 0.116m, gives a value of c_X of 43.8m/s, close to, but above the wheel unloading value. This is in part due to the fact that the displacement modes are based on the maximum instantaneous values corresponding to the calculation time step of 0.05s, rather than the 0.5s moving average value, although admittance effects will mean that the results are still filtered to some degree.

Further development of this methodology to determine these effects might at some stage prove useful.

13.3 Pantograph / OHL displacement

The roof displacement of the train having been calculated, a fairly simple extension allows the displacement between the pantograph and the overhead wire to be calculated, a parameter of importance when considering potential dewirement in high winds. The method is as follows.

- Calculate the instantaneous pantograph displacement by assuming it is a rigid body on the roof of the train that has both lateral and rotational movement.

- Calculate the overhead wire displacement at the position of the train. For the sake of simplicity it is assumed here that the displaced form of the overhead is a simple sine curve between gantries and that the displacement is proportional to the square of the three second averaged wind speed on the overhead.
- The relative displacement between the pantograph and overhead can then be calculated.

A typical result for case 2 is shown in figure 13.1 below. This shows the regular cycle of displacement between gantries, modified by the turbulent wind and dynamic train effects. The preliminary nature of this calculation must be emphasised, but it does illustrate the possibility of using the methodology in this report to study such effects.

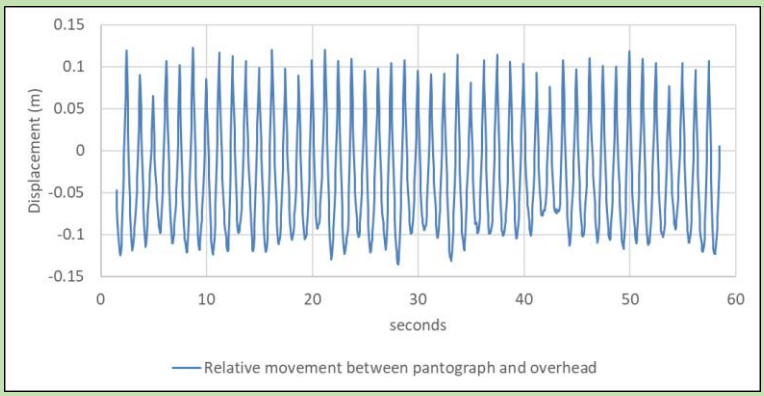

Figure 13.1 Displacement between pantograph and overhead for case 2.